Nano Res. 2011, 4(2): 180–193
DOI 10.1007/s12274-010-0068-7
Research Article

ISSN 1998-0124
CN 11-5974/O4

# Gold Supported on Metal Oxides for Carbon Monoxide Oxidation

Sonia A. C. Carabineiro[1] (✉), Nina Bogdanchikova[2], Miguel Avalos-Borja[2,†], Alexey Pestryakov[3], Pedro B. Tavares[4], and Jose L. Figueiredo[1]

[1] Laboratório de Catálise e Materiais, Associate Laboratory LSRE/LCM, Departamento de Engenharia Química, Faculdade de Engenharia, Universidade do Porto, 4200-465 Porto, Portugal
[2] Universidad Nacional Autónoma de México, Centro de Nanociencias y Nanotecnología, Carretera Tijuana-Ensenada, 22800, Ensenada, Baja California, México
[3] Tomsk Polytechnic University, 30, Lenin Avenue, Tomsk, 634050, Russia
[4] Universidade de Trás-os-Montes e Alto Douro, Centro de Química–Vila Real, Departamento de Química, 5001-911 Vila Real, Portugal
† On leave at Instituto Potosino de Investigación Científica y Tecnológica (IPICyT), San Luis Potosi, S.L.P., México

Received: 2 September 2010 / Revised: 7 October 2010 / Accepted: 28 October 2010


## ABSTRACT

Au has been loaded (1% wt.) on different commercial oxide supports (CuO, $La_2O_3$, $Y_2O_3$, NiO) by three different methods: double impregnation (DIM), liquid-phase reductive deposition (LPRD), and ultrasonication (US). Samples were characterised by $N_2$ adsorption at –196 °C, high-resolution transmission electron microscopy, selected area electron diffraction, energy dispersive X-ray spectrometry, high-angle annular dark-field imaging (Z-contrast), X-ray diffraction, and temperature programmed reduction. CO oxidation was used as a test reaction to compare the catalytic activities. The best results were obtained with Au loaded by DIM on the NiO support, with an activity of $7.2 \times 10^{-4}$ $mol_{CO} \cdot g_{Au}^{-1} \cdot s^{-1}$ at room temperature. This is most likely related to the Au nanoparticle size being the smallest in this catalyst (average 4.8 nm), since it is well known that gold particle size determines the catalytic activity. Other samples, having larger Au particle sizes (in the 2–12 nm range, with average sizes ranging from 4.8 to 6.8 nm), showed lower activities. Nevertheless, all samples prepared by DIM had activities (from $1.1 \times 10^{-4}$ to $7.2 \times 10^{-4}$ $mol_{CO} \cdot g_{Au}^{-1} \cdot s^{-1}$, at room temperature) above those reported in the literature for gold on similar oxide supports. Therefore, this method gives better results than the most usual methods of deposition–precipitation or co-precipitation.

## KEYWORDS

Gold, heterogeneous catalysis, oxidation, electron diffraction, X-ray diffraction

## 1. Introduction

The oxidation of CO to form $CO_2$ is the simplest and the most intensively studied reaction catalysed by gold [1–9]. Catalysts which promote this reaction at ambient temperatures find practical applications that include use in air-purification devices for indoor space, including gas masks, and for cleaning automotive exhaust gases. CO removal is also required in $CO_2$ lasers, and CO gas sensors are another application for gold catalysts.

Haruta and co-workers have intensively investigated

Address correspondence to sonia.carabineiro@fe.up.pt

the ability of gold to catalyse CO oxidation [1–5, 10, 11]. At the time of their early work in the 1980s, the activity for gold-supported catalysts came as a surprise [12, 13], but it is now well known that supported gold nanocatalysts are effective for CO oxidation at very low temperatures, being active even at –70 ℃ [6–9, 14, 15]. Activities do, however, depend on the choice of the metal oxide support. Although unsupported powdered gold (mean diameter 76 nm) is active for CO oxidation [16, 17], most of the studies made by Haruta and other groups have been on supported gold catalysts, with $TiO_2$, $Fe_2O_3$, and $Al_2O_3$ being the most common supports [6–9, 14, 18–23]. In this work, we wanted to use other metal oxides that have been employed to a lesser extent, namely, CuO, $La_2O_3$, NiO, and $Y_2O_3$.

The work of Tanielyan and Augustine [24], in which Au/CuO was prepared by co-precipitation (CP) under different conditions, is one of the few reports of the use of CuO as a support for CO oxidation gold catalysts. The most active catalysts were those which were heated in oxygen before use. Hutchings's group also prepared Au/CuO catalysts by CP [25, 26]. These materials were found to give sustained activity without deactivation during an 800 min experimental test [25]. Haruta used a CuO/Au composite film, prepared by the deposition of a thin CuO layer onto ultrafine Au particles for the optical detection of CO in air at around 250 ℃ [27]. CuO alone has also been rarely used as a catalyst for CO oxidation [28, 29].

Although it is considered an "active" support [19], NiO has been scarcely used for this reaction, when compared to other supports such as $TiO_2$ and $Al_2O_3$ [6–9, 15]. Haruta et al. prepared Au/NiO catalysts by CP which were very active for CO oxidation at temperatures as low as –70 ℃ [12, 30]. Behm's group also achieved good results for this type of catalyst using CP [19]. Dai and co-workers prepared highly active Au/NiO catalysts for CO oxidation using NiAu alloy nanoparticles [31]. The wet impregnation method has also been used by Radwan et al. who showed that addition of Au to NiO by this technique did not improve catalytic activity [32]. Other publications have also shown the good properties of Au/NiO catalysts [33–35]. In addition, NiO nanorings (without gold) showed an unexpected catalytic property for CO oxidation [36].

To the best of our knowledge, the only work reported in the literature on the use of $Y_2O_3$ as a support for gold is from Corma's group [37, 38]. In fact, this oxide, considered an "inadequate" support for Au catalysts, was transformed into a highly active material when Au was deposited on nanocrystalline $Y_2O_3$ particles, instead of being prepared by a conventional precipitation method.

$La_2O_3$ is another example of a rarely used support. $Au/La_2O_3$ catalysts were obtained by precipitation techniques, and shown to be more active for CO oxidation when compared with $Au/CeO_2$ and $Au/ZrO_2$ prepared in the same way [39]. $La_2O_3$-supported Au(III) complexes synthesized from an $Au(CH_3)_2(C_5H_7O_2)$ [$C_5H_7O_2$ = acetylacetonate] precursor were also shown to be highly active and stable CO oxidation catalysts at room temperature, not suffering from deactivation even after 50 h of continuous operation in a flow reactor [40, 41]. The authors found that supported gold nanoparticles were readily oxidized by $CO_2$, suggesting that $CO_2$ could be the actual oxidant of gold in CO oxidation catalysis [41, 42].

As traditional deposition–precipitation (DP) [6–9, 15, 26, 43–45] and CP [6–9, 12, 13, 15, 19, 24–26, 29] are the most common methods to prepare oxide-supported gold catalysts, we wanted to combine the use of unusual supports with unusual methods, such as double impregnation (DIM) [46], and liquid-phase reductive deposition (LPRD) [47], in order to prepare Au nanoparticles. To the best of our knowledge, the only reports of the use of DIM are the work of Bowker et al. dealing with $TiO_2$ samples [46] and our previous work on $CeO_2$ [48, 49] and ZnO [50] catalysts. This method represents an environmentally and economically more favourable route to high activity gold catalyst production, when compared with the traditional DP method [46]. As far as we know, LPRD has only been used by Sunagawa et al. to prepare Pt and Au catalysts on $Fe_2O_3$, FeOOH, $ZrO_2$, and $TiO_2$ supports [47], and by us to prepare $Au/CeO_2$ [51] and $Au/TiO_2$ [52] catalysts. Ultrasonication (US) has only previously been used by our group to prepare highly active Au/ZnO materials [50]. In these methods, a washing procedure is carried out in order to eliminate residual chloride, which is well known to cause sintering of Au nanoparticles, thus rendering them inactive [6–9].

In this work, a comparison of the physicochemical properties of gold nanoparticles supported on different oxides (CuO, $La_2O_3$, NiO, and $Y_2O_3$), prepared by the methods described above (DIM, LPRD, and US), is presented. Samples were tested as catalysts for the oxidation of CO, which is a simple established model reaction to evaluate gold catalysts with many potential applications, but which is not yet fully understood, in spite of being intensively studied [6–9, 14]. A comparison is made with $Au/CeO_2$ and $Au/TiO_2$ catalysts also prepared by the DIM method.

## 2. Experimental

### 2.1 Oxide supports

The following commercial supports were tested: CuO (powder, purum, Riedel-de Haën), NiO (black, < 10 μm, Aldrich), $La_2O_3$ (99.99% metals basis, Aldrich), and $Y_2O_3$ (Art. 12412, Merck). These oxides were used both as received and after treatment at 400 °C in $N_2$ for 2 h (hereafter referred as "treated"). $CeO_2$ (Fluka) and $TiO_2$ P25 (Evonik Degussa) were also used for comparison.

### 2.2 Preparation of Au catalysts

Au was loaded on the oxide supports by DIM [46], LPRD [47], and US [50]. Briefly, DIM involves impregnating the support with an aqueous solution of the gold precursor and then with a solution of $Na_2CO_3$ [46, 48–50]. LPRD involves mixing a solution of $HAuCl_4$ with a solution of NaOH (with a ratio of 1:4 by mass) [47, 51, 52]. US involves dissolving the Au precursor in water and methanol, and sonicating for 8 h [50]. Further details can be found elsewhere [46–52].

### 2.3 Characterization techniques

The materials were analysed by adsorption of $N_2$ at –196 °C, in a Quantachrome NOVA 4200e apparatus. Temperature programmed reduction (TPR) and temperature programmed desorption (TPD) experiments were performed in a fully automated AMI-200 Catalyst Characterization Instrument (Altamira Instruments), equipped with a quadrupole mass spectrometer (Dymaxion 200 amu, Ametek). Further details can be found elsewhere [48, 49, 51, 53]. Conventional transmission electron microscopy (TEM) measurements were performed with a JEOL 2010 microscope with a point-to-point resolution better than 0.19 nm. High resolution transmission electron microscopy (HRTEM), energy-dispersive X-ray spectroscopy (EDXS), and Z-contrast measurements were done on a FEI Tecnai F30 instrument. The Z-contrast images were collected using a high-angle annular dark-field detector (HAADF), in scanning transmission mode (STEM). The sample was mounted on a carbon polymer-supported copper micro-grid. A few droplets of a suspension of the ground catalyst in isopropyl alcohol were placed on the grid, followed by drying under ambient conditions. The average gold particle size and the particle size distribution were determined from measurements made on ~100–300 particles, depending on the sample. Simulations and fitting of selected area electron diffraction (SAED) patterns were carried out with the "JEMS" software [54]. X-ray diffraction (XRD) analysis was carried out in a PANalytical X'Pert MPD equipped with a X'Celerator detector and secondary monochromator (Cu $K\alpha$ $\lambda$ = 0.154 nm, 50 kV, 40 mA; data recorded at a 0.017° step size, 100 s/step). Rietveld refinement with PowderCell software [55] was used to identify the crystallographic phases present and to calculate the crystallite size from the XRD diffraction patterns. Semi-quantitative estimation of gold loading was performed by EDXS. Further details can be found elsewhere [48–52].

### 2.4 Catalytic tests

Catalytic activity measurements were performed for CO oxidation, using a continuous-flow reactor. The catalyst sample (0.2 g) was placed on a quartz wool plug in a 45 cm long silica tube with 2.7 cm i.d., inserted into a vertical furnace equipped with a temperature controller. Feed gas (5% CO, 10% $O_2$ in He) was passed through the catalytic bed at a total flow rate of 50 $cm^3 \cdot min^{-1}$ (in contrast with most literature studies that use 1% CO or less [6–9, 15]). The composition of the outgoing gas stream was determined using a gas chromatograph equipped with a capillary column (Carboxen-1010 PLOT, Supelco) and a thermal conductivity detector. The activity results were obtained after the steady state was reached. Further details can be found elsewhere [48–52].

## 3. Results and discussion

### 3.1 Characterization of samples

#### 3.1.1 *Brunauer–Emmett–Teller (BET) surface area*

Table 1 shows the characterisation results for the oxide supports obtained by $N_2$ adsorption at –196 ˚C. Thermal treatment lowered the BET surface area of NiO from 70 to 32 $m^2$/g. A decrease was also observed for CuO, but the surface areas are very small (5–11 $m^2$/g). The remaining oxides maintained their BET surface areas after the thermal treatment. The values are within those reported in literature for similar oxides of Cu and Ni [29, 30, 36]. Smaller values were obtained in this work for $Y_2O_3$ and $La_2O_3$ supports, when compared with the Ref. [37, 39–42, 56–58]. Addition of gold to the oxides, by any of the methods, did not produce significant changes in the BET surface areas, as seen in Table S-1 in the Electronic Supplementary Material (ESM).

#### 3.1.2 *XRD*

Figure 1 shows the XRD results obtained for the oxide supports alone (as received), and loaded with 1% wt. Au by DIM. As can be seen in Fig. 1 and Table 1, the identified phases for the unloaded materials are the respective oxides, as expected, with the exception of $La_2O_3$ in which $La(OH)_3$ was found. This phase was also detected in the unsupported and supported $La_2O_3$ catalysts by other authors and is formed mostly by the hydrolysis of $La_2O_3$ during the exposure of the catalysts to atmospheric moisture [59]. In our study, this phase was also detected in the thermally treated sample, showing that thermal treatment at 400 ˚C for up to 24 h does not change the phase content.

The crystallite size of CuO is similar to that found by Radwan et al., with or without Au [32]. It is, however, much smaller than that found for another commercial CuO sample (Alfa Aesar: 115 nm) by Pillai and Deevi [29]. However, the same authors achieved smaller particle size (16 nm) by preparing a CuO sample by precipitation of copper nitrate [29].

The value for the commercial $Y_2O_3$ we used in this work (43 nm) is however, much larger than that found by Corma and co-workers for $Y_2O_3$ powder (27 nm) [37] and nanocrystalline $Y_2O_3$ (~6 nm) [37, 38]. The same is also true for the $La_2O_3$ we used (23 nm), compared with the literature value for $La_2O_3$ synthesized by base hydrolysis of lanthanum nitrate with NaOH in the presence of acetic acid (12 nm) [41].

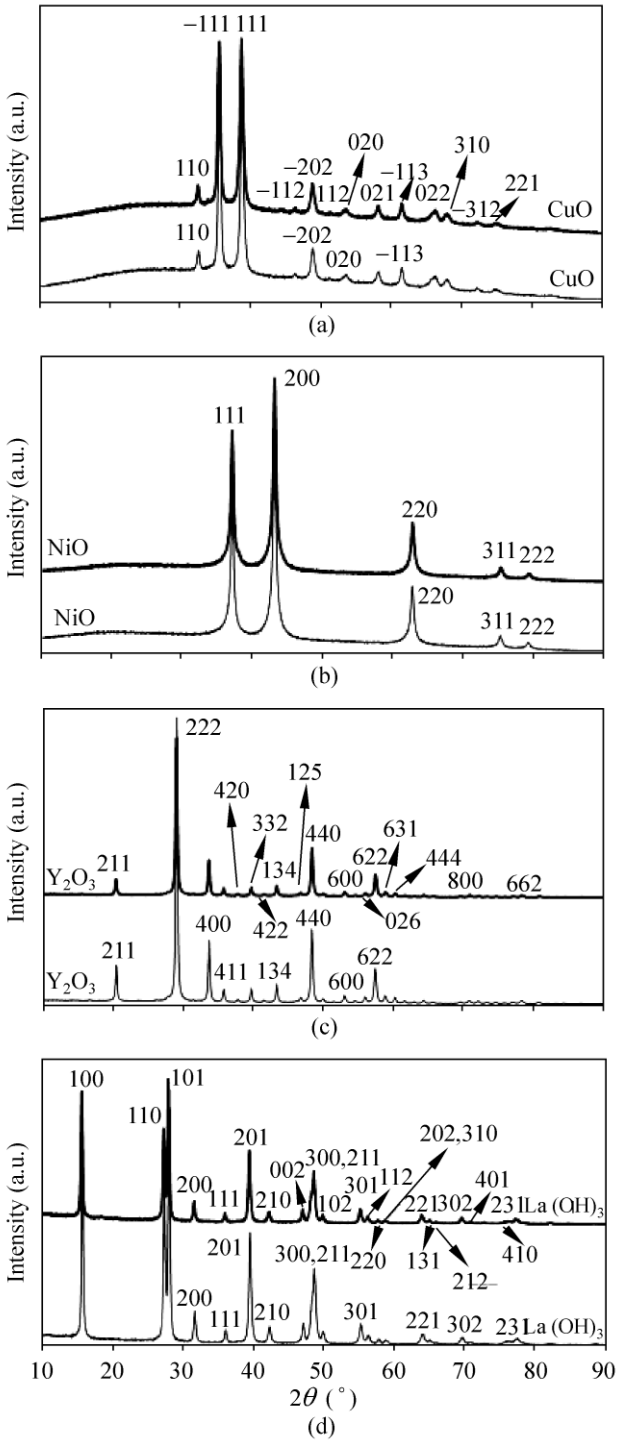


**Figure 1** X-ray diffraction patterns of commercial CuO (a), NiO (b), $Y_2O_3$ (c), $La_2O_3$ (d), as received (lower pattern) and loaded with 1% wt. Au by DIM (upper pattern), with phases and respective crystal planes (Miller indexes) identified

**Table 1** BET surface areas of the oxide samples obtained by adsorption of $N_2$ at –196 °C, crystallite sizes and phases detected by XRD

| Metal oxide sample | BET area ($m^2$/g) | Phase detected (crystal system, space group, reference code in database) | Crystallite size (nm) |
|---|---|---|---|
| CuO | 11 | CuO (monoclinic *C*2/*c*, 01-080-0076) | 25 |
| CuO (treated) | 5 | – | – |
| NiO | 79 | NiO (cubic *Fm*-3*m*, 00-047-1049) | 26 |
| NiO (treated) | 32 | – | – |
| $Y_2O_3$ | 9 | $Y_2O_3$ (cubic, *Ia*-3, 01-083-0927) | 43 |
| $Y_2O_3$ (treated) | 8 | – | – |
| $La_2O_3$ | 11 | $La(OH)_3$ (hexagonal, $P6_3/m$, 01-083-2034) | 23 |
| $La_2O_3$ (treated)[a] | 10 | $La(OH)_3$ (hexagonal, $P6_3/m$, 01-083-2034) | – |

[a] Thermally treated for 24 h at 400 °C in $N_2$

The Au particle size could not be determined for any of the samples by XRD analysis, since the characteristic XRD reflection was absent in these materials. This is due to the low loading (1% wt.) and small size (as shown by HRTEM) of the Au particles present in these catalysts, and is consistent with the observations of other authors for Au/CuO catalysts [26].

### 3.1.3 *HRTEM/HAADF/EDXS*

Supports alone (untreated) and loaded with Au were analysed by HRTEM. Since the samples prepared by US were found to be less active for CO oxidation (see below), only samples prepared by DIM and LPRD were further characterised. EDXS confirmed the presence of gold (~1% wt. Au) for all samples.

Figure 2 shows images of the supports. It can be observed that the commercial CuO support (Fig. 2(a)) consists of a mixture of filament-like particles with average diameter of 20 nm and with lengths ranging from 20 to 150 nm. Larger round particle agglomerates of ~200 nm diameter are also present. The commercial sample of NiO (Fig. 2(b)) consists of a mixture of particles of several different sizes ranging from 5 to 100 nm. Interestingly, ~2.9% of "free carbon" was detected by EDXS (Fig. S-1 in the ESM), and thermogravimetry showed the presence of 2.5% carbon (Fig. S-2 in the ESM) in this material. $Y_2O_3$ (Fig. 2(c)) shows some interesting parallelepiped-like structures with sizes ranging from 10 to 90 nm. Finally, $La_2O_3$ (Fig. 2(d)) contains large agglomerates of particles ranging in size from ~300 to ~500 nm.

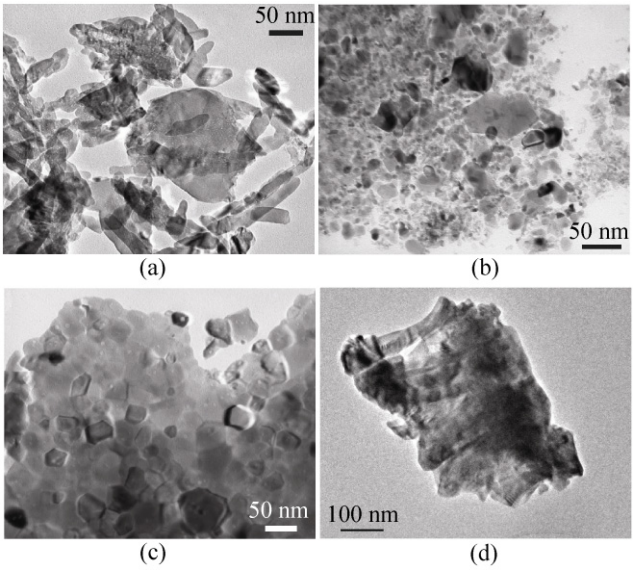


**Figure 2** HRTEM images of the commercial supports: CuO (a), NiO (b), $Y_2O_3$ (c), and $La_2O_3$ (d)

HRTEM and HAADF results of supports loaded with Au are shown in Fig. 3. Gold particles are seen as darker spots in HRTEM and as bright dots in HAADF images. Figures 3(a) and 3(b) show representative HRTEM results for CuO with Au loaded by DIM and LPRD, respectively. Analysing the size distribution histogram of gold nanoparticles on this support (Figs. 4(a) and 4(b)), taken from several HRTEM images, it can be seen (Table 2) that although the gold size range for the two samples is the same (2–12 nm), the DIM sample has an average gold size which is smaller (5.8 nm) than the LPRD sample (6.6 nm). Larger Au particles were observed by Hutchings et al.

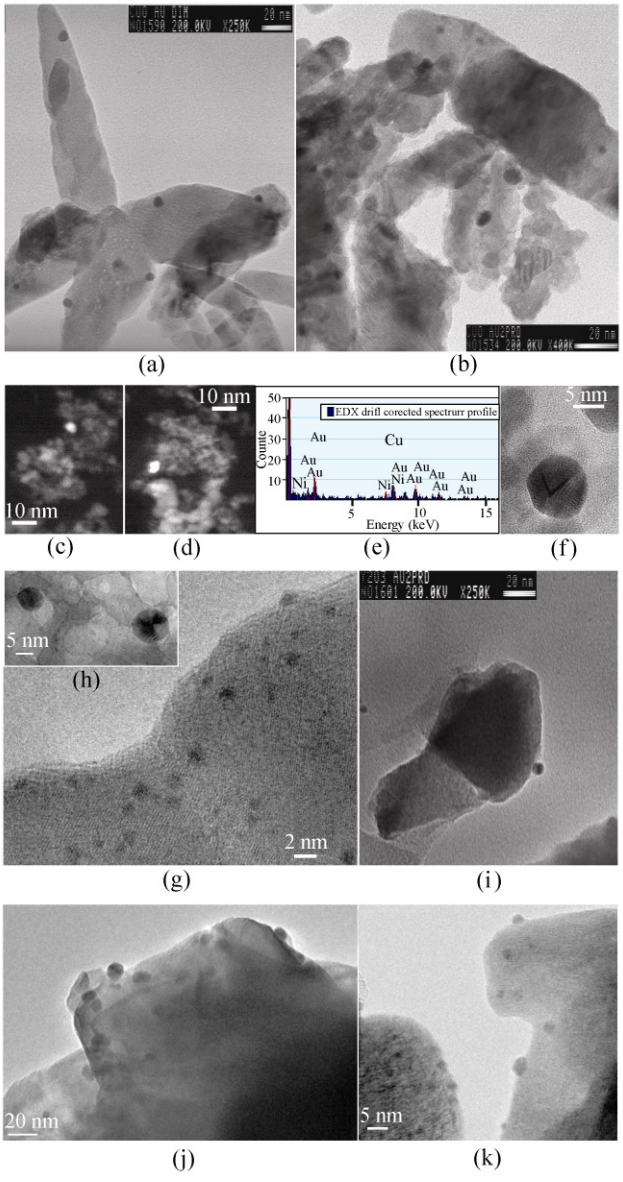


**Figure 3** HRTEM images of CuO with Au loaded by DIM (a) and LPRD (b). HAADF images of NiO with Au loaded by DIM (c) and LPRD (d). EDXS spectrum (e) taken on a bright dot (gold particle) and HRTEM image of "treated" NiO with Au loaded by LPRD (f). HRTEM images of $Y_2O_3$ with Au loaded by DIM (g), showing a closer detail of Au nanoparticles as inset (h), and by LPRD (i). HRTEM images of $La_2O_3$ with Au loaded by DIM (j) and LPRD (k)

for Au/CuO catalysts prepared by CP, where the mean Au particle size was 20–30 nm, and there were many particles as large as 50 nm [25]. In contrast, Ko et al. obtained a Au/CuO sample prepared by DP from $Cu(OH)_2$ with an average gold particle size of 3.8 ± 0.5 nm [60].

**Table 2** Average gold nanoparticle sizes and size ranges for the Au/oxide samples prepared by DIM and LPRD

| Au/oxide | Gold size range (nm) | Average gold particle size (nm) |
|---|---|---|
| Au/CuO (DIM) | 2–12 | 5.8 |
| Au/CuO (LPRD) | 2–12 | 6.6 |
| Au/NiO (DIM) | 2–8 | 4.8 |
| Au/NiO (LPRD) | 2–11 | 5.4 |
| Au/$Y_2O_3$ (DIM) | 2–10 | 5.5 |
| Au/$Y_2O_3$ (LPRD) | 2–12 | 6.8 |
| Au/$La_2O_3$ (DIM) | 2–12 | 5.9 |
| Au/$La_2O_3$ (LPRD) | 2–12 | 6.1 |

Au/NiO samples were also analysed by HRTEM. In this case, however, the gold particles could not be identified, as the images look very similar to those obtained for the support alone (as seen in Figs. S-3 and S-4 in the ESM). This is due to the presence of free carbon on the support, as mentioned above (as seen in Figs. S-5 and S-6 in the ESM). Therefore HAADF was used in an attempt to image the gold particles. This technique is highly sensitive to variations in the atomic number of atoms in a sample, allowing Z-contrast images to be formed [48, 49, 51, 61]. In Figs. 3(c) and 3(d), gold particles supported on NiO prepared by DIM and LPRD, respectively, are seen as bright spots. Figure 3(e) shows an EDXS spectrum of one of the selected bright areas, confirming the presence of gold. When the sample was treated at 400 ˚C, some carbon was removed and gold particles were then easily seen by HRTEM (an example is shown in Fig. 3(f)). However, the treated samples were not as active for CO oxidation as the untreated ones, as will be discussed below. In addition, an attempt to synthesise NiO by an exotemplating method, similar to what was performed for $CeO_2$ [49] and $MnO_2$ [53] materials, was carried out. This sample, consisting of NiO prepared with a carbon template that was removed by calcination, was much less active than the commercial oxide, with or without Au. This means that the carbon found in commercial NiO must be related to its high activity. Further research is needed to clarify this point. The Au/NiO sample prepared by DIM in this work (with the commercial support) showed a narrower size distribution (2–8 nm) and a smaller average gold particle size of 4.8 nm (Fig. 4(c)

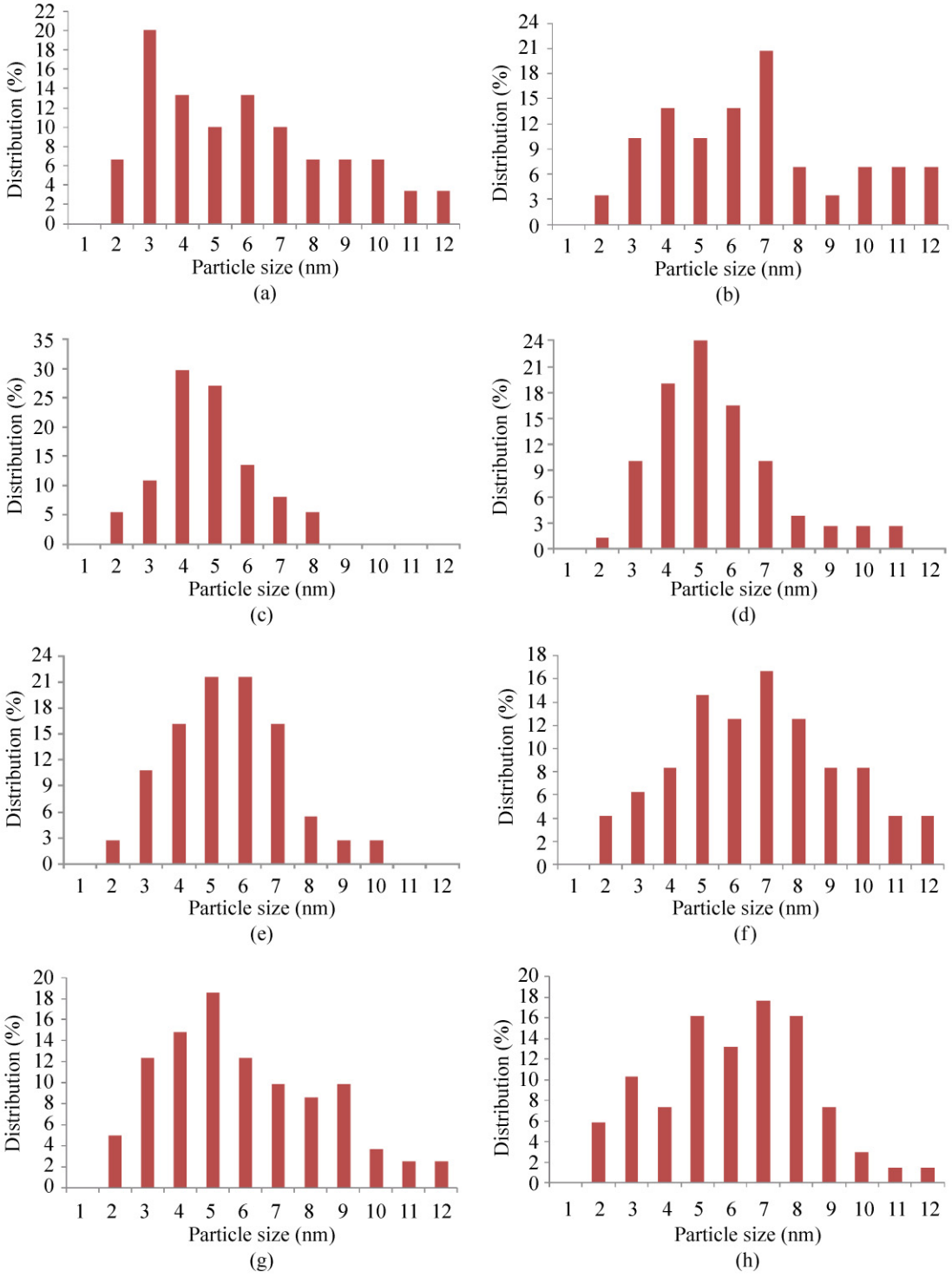


**Figure 4** Size distribution histograms of gold nanoparticles on CuO with Au loaded by DIM (a) and LPRD (b), NiO with Au loaded by DIM (c) and LPRD (d), $Y_2O_3$ with Au loaded by DIM (e) and LPRD (f), and $La_2O_3$ with Au loaded by DIM (g) and LPRD (h)

and Table 2), when compared to the LPRD material (Fig. 4(d) and Table 2). These are smaller than those found by Haruta et al. for Au/NiO catalysts prepared by CP and DP (~8 nm) [13, 62], but similar to the value of 3.2 ± 1 nm reported by Behm and co-workers using the same method [19].

The gold particles are clearly visible on the $Y_2O_3$ support. Figures 3(g) and 3(h) show the sample with Au loaded by DIM, in a general view and in closer detail, respectively. In Fig. 3(i), a detail of a piece of the support is seen with one gold particle on the right-hand side. The $La_2O_3$ support with Au loaded by DIM (Fig. 3(j)) and LPRD (Fig. 3(k)) also yielded nice HRTEM images. The histograms (Figs. 3(e)–3(h)) show that the size range varies from 2 to 12 nm (Table 2), as with the CuO samples. In general, the DIM method produced smaller particles for all materials.

Gold nanoparticles of smaller size (4 nm) were found by Guzman and Corma on nanocrystalline $Y_2O_3$ [37]. As for the literature concerning $La_2O_3$, a 2% wt. $Au/La_2O_3$ catalyst obtained by precipitation yielded a cluster size of 1–4 nm for the as-prepared catalyst [39]. However, sintering occurred at 800 °C, and the Au particle size increased, ranging between 20 and 40 nm [39]. Haruta and co-workers reported that gold nanoparticles smaller than 8 nm could be prepared on $La(OH)_3$ using CP [62].

### 3.1.4 SAED

Figure 5 shows the SAED images obtained for the untreated oxides with gold loaded by DIM. The simulations are shown for monoclinic CuO (Fig. 5(a)) and cubic Au (Fig. 5(b)) for the Au/CuO sample. Cubic NiO (Fig. 5(c)) and cubic Au (Fig. 5(d)) match well with the results for Au/NiO. Cubic $Y_2O_3$ (Fig. 5(e)) and cubic Au (Fig. 5(f)) were simulated for the $Au/Y_2O_3$ sample. The adjustment for cubic gold on $Y_2O_3$ (Fig. 5(f)) is not so clear; however the HRTEM and EDXS results showed the presence of gold. Finally, hexagonal $La(OH)_3$ (Fig. 5(g)) and cubic Au (Fig. 5(h)) were fitted for $Au/La_2O_3$. It was found that $La_2O_3$ did not adjust in this case. The results obtained match very well with those obtained by XRD (except that Au was not detected by this latter technique, as mentioned earlier).

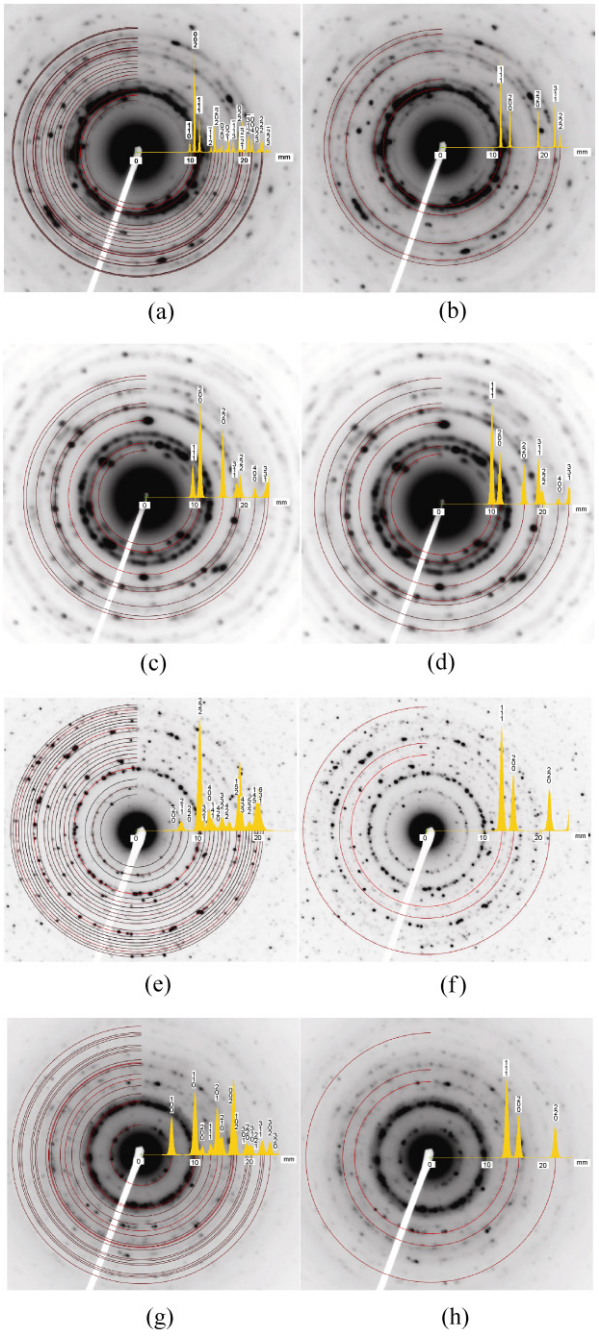


**Figure 5** SAED images of CuO (a, b), NiO (c, d), $Y_2O_3$ (e, f), and $La_2O_3$ (g, h) with gold loaded by DIM. The images show the simulations for monoclinic CuO (a) and cubic Au (b) for Au/CuO sample; cubic NiO (c) and cubic Au (d) for Au/NiO; cubic $Y_2O_3$ (e), and cubic Au (f) for Au/ $Y_2O_3$; and hexagonal $La(OH)_3$ (g) and cubic Au (h) for Au/ $La_2O_3$

### 3.1.5 TPR

TPR results are shown in Figs. 6(a)–6(d), for the as-received commercial supports, and after loading with gold by DIM. One major peak is seen in the TPR

of the CuO sample at ~300 ℃, with a shoulder at ~244 ℃ (Fig. 6(a)). After the addition of gold, the peak temperatures decreased slightly to ~295 ℃ and ~238 ℃. According to the literature, two reduction peaks are expected for CuO, with or without Au, around ~200 ℃, which correspond to the CuO → $Cu_2O$ and $Cu_2O$ → Cu transitions [26].

Typical TPR spectra of NiO samples exhibit a main peak in the range 220–370 ℃ which is due to the $Ni^{2+}$ → $Ni^0$ transition [63–66]. In our case (Fig. 6(b)), a major peak is observed at ~340 ℃, with a shoulder at ~250 ℃. After the addition of gold, these temperatures decreased to ~297 ℃ and ~215 ℃, respectively. Some authors have attributed the peak at lower temperature to non-stoichiometric surface oxygen and the other one to non-stoichiometric bulk oxygen in the oxide [65].

Figure 6(c) shows the TPR spectra of $Y_2O_3$, with and without Au. A very small peak is observed at ~500 ℃, in both cases. A small peak at ~630 ℃ has been reported by other authors for $Y_2O_3$ prepared from yttrium nitrate [67].

Negative TPR peaks were found for the $La(OH)_3$ (as noted above, lanthanum hydroxide was present instead of the expected oxide) materials as can be seen in Fig. 6(d), with or without gold, indicating no consumption of hydrogen. Again, water release was detected by mass spectrometry (MS), most likely meaning that $La_2O_3$ is being formed ($La(OH)_3$ → $La_2O_3 + H_2O$). In fact, a second TPR run produced the characteristic $La_2O_3$ trace, showing several small positive peaks, found in the literature for the oxide [39].

### 3.2 Catalytic tests

It was found that the activity for CO oxidation (with or without Au) of the thermally treated oxides did not improve when compared with the as-received samples; in fact, thermal treatment was detrimental in some cases. Therefore, only the results for the untreated samples are shown in Fig. 7. Before loading with Au, NiO, and CuO were the most active supports, achieving full conversion of CO at ~150 ℃, in contrast with results from previous authors reporting no conversion of CO for CuO at room temperature [26]. Figures 7(a) and 7(b) show that NiO was slightly more active than CuO at room temperature. In fact, other authors have shown that NiO nanorings exhibited unexpected catalytic activity for CO oxidation [36]. The other supports (Figs. 7(c)–7(e)) only achieved full conversion of CO at ~650–700 ℃; however, $Y_2O_3$ had a better performance than $La(OH)_3$ between 200 ℃ and 600 ℃.

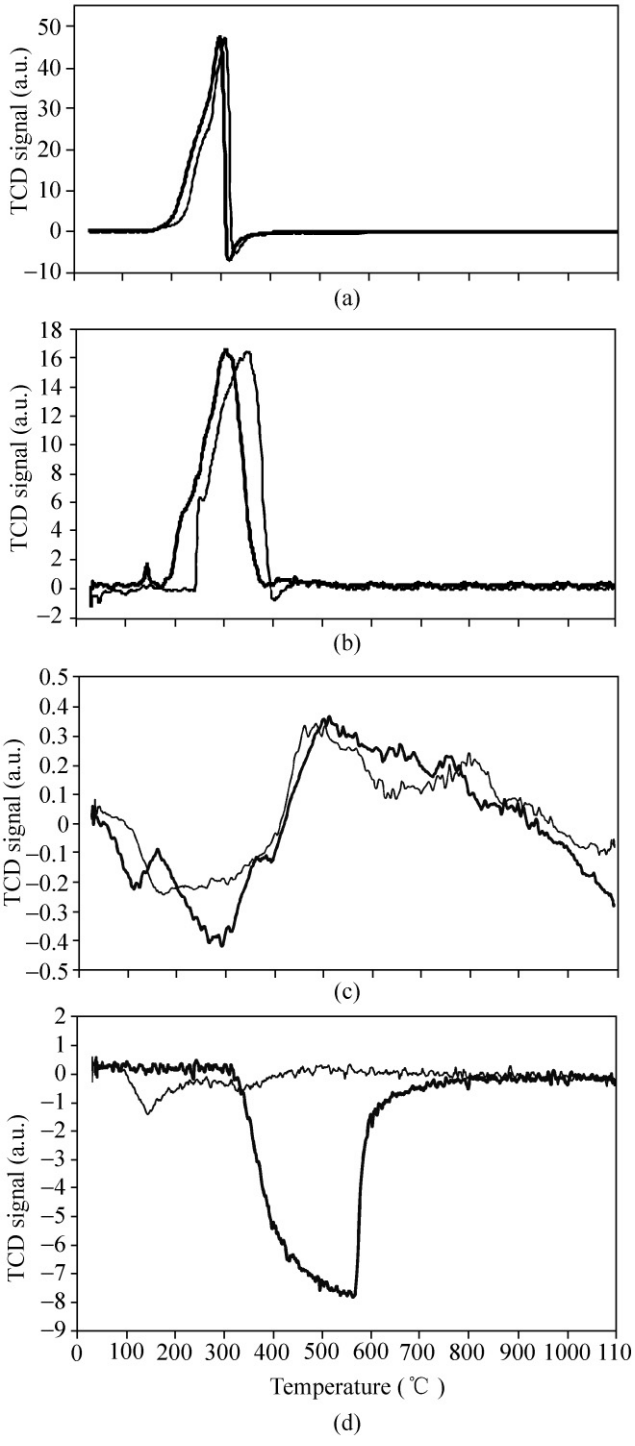


**Figure 6** $H_2$-TPR profiles of the commercial CuO (a), NiO (b), $Y_2O_3$ (c), and $La_2O_3$ (d), as received (thin lines) and loaded with 1% wt. Au by DIM (thicker lines)

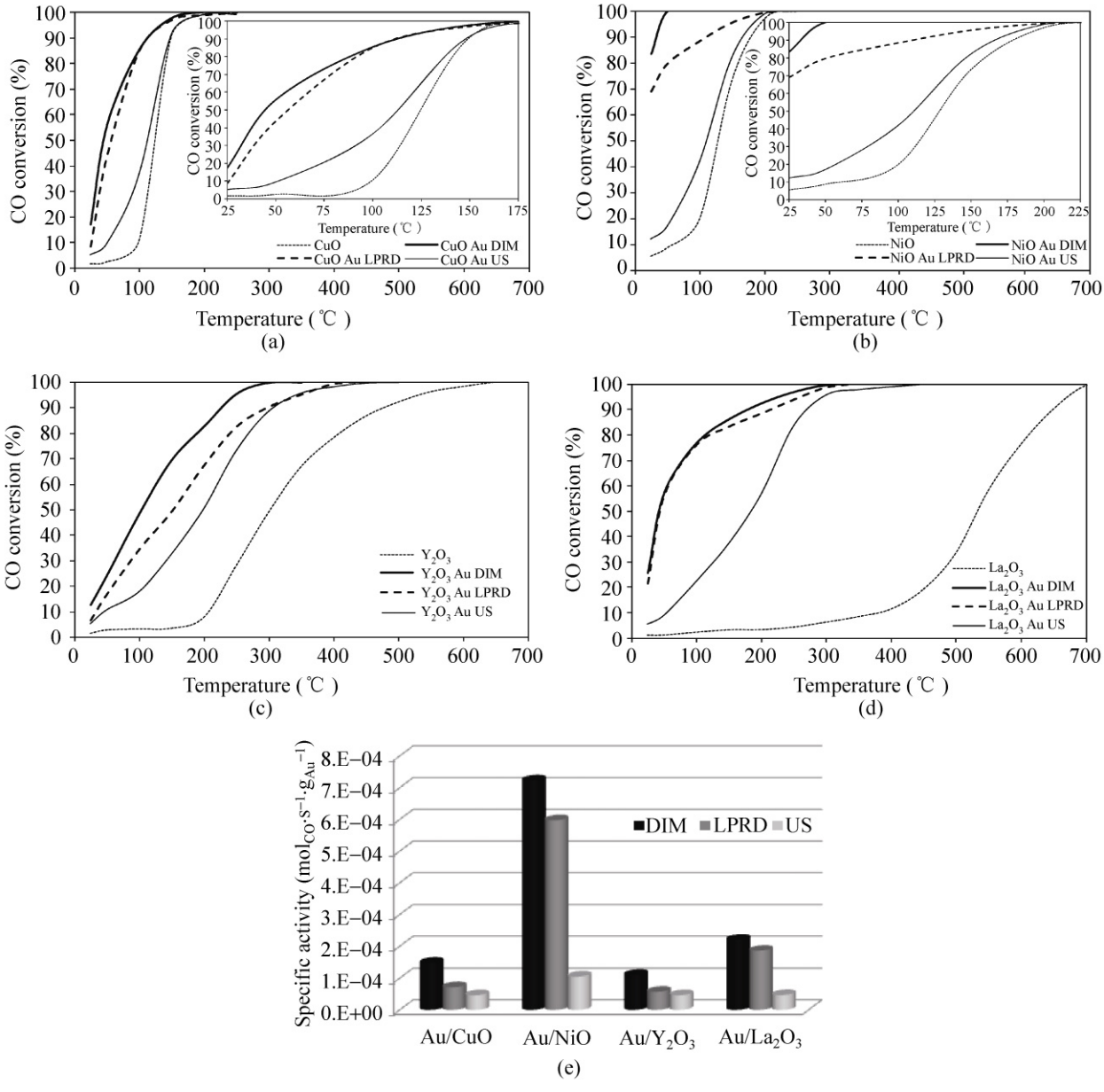


**Figure 7** Plots of CO conversion (%) versus temperature for the CuO (a), NiO (b), $Y_2O_3$ (c), and $La_2O_3$ (d) supports alone and with Au loaded by different methods. Figures (a) and (b) have insets which show details at low temperature. Specific activities for the different Au/oxide catalysts determined at room temperature are shown in (e)

As expected, loading the samples with Au resulted in CO total conversion occurring at much lower temperatures than with the supports alone. DIM was found to be the best gold loading method. For CuO (Fig. 7(a)) and $La_2O_3$ (Fig. 7(e)), LPRD gave catalysts showing similar behaviour. For $Y_2O_3$ (Fig. 7(c)), the catalytic activity was similar for materials prepared by DIM and LPRD, but at higher temperatures DIM gave materials with a better performance. For NiO, DIM is undoubtedly better than LPRD, with the catalyst achieving a conversion as high as 85% at room temperature, and full conversion at 50 ℃; therefore, this sample is the most active found in this study. US was found to be the worst gold loading method for these supports, in contrast with the results found in our previous work with Au/ZnO catalysts [50].

Some gold catalysts described in the literature give full CO conversion at room temperature, but it has to be taken into account that most studies in the literature use 1% CO or less [6–9] (while we used 5% CO). In addition, most studies use higher loadings of Au [6–9] (while we used 1% wt.). Nevertheless, it is possible to see, in our case, that CO conversion at room temperature increased by up to 20 times on addition of gold (for the NiO and $La_2O_3$ with Au loaded by DIM), when compared to the unloaded samples.

The activities obtained at room temperature for our Au/CuO materials varied from 0.17 to 0.53 $mol_{CO}·g_{Au}^{-1}·h^{-1}$ (that is, $4.6 × 10^{-5}$ and $4.5 × 10^{-4}$ $mol_{CO}·g_{Au}^{-1}·s^{-1}$, as seen in Fig. 7(e), for the samples with Au loaded by US and DIM respectively), which is higher than the value reported by Solsona et al. at 25 ℃ for a Au/CuO catalyst prepared by CP (0.09 $mol_{CO}·g_{Au}^{-1}·h^{-1}$) [26].

Schubert et al. reported a value of $20 × 10^{-4}$ $mol_{CO}·g_{Au}^{-1}·s^{-1}$ at 80 ℃ for a Au/NiO catalyst prepared by CP [19]. This value cannot be compared with our DIM catalyst since it achieved full conversion at 50 ℃ (however, at room temperature, the value obtained was already $7.2 × 10^{-4}$ $mol_{CO}·g_{Au}^{-1}·s^{-1}$ as seen in Fig. 7(e)). Our other Au/NiO catalysts prepared by US and LPRD were less active, showing values of $3.6 × 10^{-4}$ $mol_{CO}·g_{Au}^{-1}·s^{-1}$ and $7.7 × 10^{-4}$ $mol_{CO}·g_{Au}^{-1}·s^{-1}$ at 80 ℃, respectively (Fig. 7(e)).

Guzman and Corma [37] reported that the specific rate per gram of Au of a catalyst prepared with nanocrystalline $Y_2O_3$ was $2.1 × 10^{-4}$ $mol_{CO}·g_{Au}^{-1}·s^{-1}$ at 50 ℃. Our Au/$Y_2O_3$ catalyst prepared by DIM showed an activity of $2.2 × 10^{-4}$ $mol_{CO}·g_{Au}^{-1}·s^{-1}$ at room temperature (Fig. 7(e)), which is a comparable value, especially considering that Guzman and Corma used nanocrystalline $Y_2O_3$, and that they obtained negligible activity for Au supported on a commercial $Y_2O_3$ material at the same temperature.

Russo et al. reported total CO conversion at ~225 ℃ (for 2% wt. Au supported on a $La_2O_3$ catalyst, using a mass of 800 mg and 2300 ppm CO) [39]. At that same temperature, our conversions were 90%–95% for the catalysts prepared by LPRD and DIM (Fig. 7(d)), which is remarkable, considering that our catalysts contained 1% wt. Au, and that we used a mass of 200 mg, and 5% CO in the feed.

In order to compare the results obtained with the DIM method for the supports used in this work with more common supports in literature, such as $CeO_2$ and $TiO_2$, additional CO oxidation tests were carried out for Au/$CeO_2$ and Au/$TiO_2$ samples prepared by DIM. The variation of CO conversion with temperature can be found in Figs. S-7 and S-8, respectively, in the ESM. The activity for Au on $TiO_2$ prepared by DIM was very low (in fact, negligible below 100 ℃), when compared with that of the CuO, NiO, $Y_2O_3$, and $La_2O_3$ materials loaded with gold by the same method. Au/$CeO_2$ was more active than Au/$TiO_2$, achieving 38% CO conversion at low temperature [48], however Au/NiO DIM was still more active, since 85% conversion was found at room temperature, as discussed above.

## 4. Conclusions

1% wt. Au has been loaded on less commonly used commercial oxide supports (CuO, $La_2O_3$, $Y_2O_3$, NiO) by three different unusual methods: DIM, LPRD, and US.

Low BET surface areas were found for the oxide supports, as expected, which did not vary much after gold addition. Gold particle sizes from 2–12 nm were detected, with average sizes ranging from 4.8 to 6.8 nm.

The best results for CO oxidation were obtained for the NiO support with Au loaded by DIM, showing an activity of $7.2 × 10^{-4}$ $mol_{CO}·g_{Au}^{-1}·s^{-1}$ at room temperature. This is most likely related to it having the lowest Au nanoparticle size (an average of 4.8 nm), since it is well known that the Au particle size mostly determines catalytic activity. It was found that the commercial sample of NiO contained about 2.5% carbon, which prevented visualisation of gold particles by HRTEM, but they could be observed by HAADF. The removal of carbon by heating allowed the gold particles to be seen by HRTEM, but was detrimental to catalytic activity. Further research needs to be carried out on this subject.

Other samples, having larger Au particle sizes, showed lower activities for CO oxidation. Nevertheless, all samples prepared by DIM showed activities (from $1.1 × 10^{-4}$ to $7.2 × 10^{-4}$ $mol_{CO}·g_{Au}^{-1}·s^{-1}$, at room temperature) above those reported in the literature so far for gold on similar oxide supports. This shows that

this method (DIM) gives better results than the traditional methods like deposition–precipitation or co-precipitation.

## Acknowledgements

The authors thank Fundação para a Ciência e a Tecnologia (FCT), Portugal, for financial support (CIENCIA 2007 program for Sónia Carabineiro (SAC)), and project PTDC/EQU-ERQ/101456/2008, financed by Fundação para a Ciência e Tecnologia (FCT) and FEDER in the context of Programme COMPETE. Funds from Mexican Consejo Nacional de Ciencia y Tecnologia (CONACYT) grant No. 79062 and Programa de Apoyo a Proyectos de Investigación e Innovación Tecnológica (PAPIT-UNAM) grant No. IN 100908 are also acknowledged. The authors thank Laboratorio de Investigaciones en Nanociencias y Nanotecnologia (LINAN) laboratory from IPICyT for providing microscopy and simulation services for this work.

**Electronic Supplementary Material**: Supplementary material (characterisation of oxide samples loaded with Au, EDXS, and thermogravimetry/differential scanning calorimetry (TG/DSC) results for the commercial NiO sample, HRTEM images of NiO with Au loaded by DIM and LPRD, CO conversion (%) versus temperature for the $CeO_2$ and $TiO_2$ commercial supports alone and with Au loaded by DIM) is available in the online version of this article at http://dx.doi.org/10.1007/s12274-010-0068-7.



## References

[1] Haruta, M. Size- and support-dependency in the catalysis of gold. *Catal. Today* **1997**, *36*, 153–166.

[2] Haruta, M.; Date, M. Advances in the catalysis of Au nanoparticles. *Appl. Catal. A: Gen.* **2001**, *222*, 427–437.

[3] Haruta, M. Catalysis of gold nanoparticles deposited on metal oxides. *Cattech* **2002**, *6*, 102–115.

[4] Haruta, A. When gold is not noble: Catalysis by nanoparticles. *Chem. Rec.* **2003**, *3*, 75–87.

[5] Haruta, M. Gold as a novel catalyst in the 21st century: Preparation, working mechanism, and applications. *Gold. Bull.* **2004**, *37*, 27–36.

[6] Bond, G. C.; Thompson, D. T. Gold-catalysed oxidation of carbon monoxide. *Gold. Bull.* **2000**, *33*, 41–51.

[7] Bond, G. C.; Louis, C.; Thompson, D. T. *Catalysis by Gold*; Imperial College Press: London, United Kingdom, 2006.

[8] Carabineiro, S. A. C.; Thompson, D. T. Catalytic Applications for Gold Nanotechnology. In *Nanocatalysis*. Springer-Verlag: Berlin, Heidelberg, New York, 2007.

[9] Carabineiro, S. A. C.; Thompson, D. T. Gold Catalysis. In *Gold: Science and Applications*. CRC Press, Taylor and Francis Group: Boca Raton, London, New York, 2010.

[10] Hutchings, G. J.; Haruta, M. A golden age of catalysis: A perspective. *Appl. Catal. A: Gen.* **2005**, *291*, 2–5.

[11] Date, M.; Imai, H.; Tsubota, S.; Haruta, M. *In situ* measurements under flow condition of the CO oxidation over supported gold nanoparticles. *Catal. Today* **2007**, *122*, 222–225.

[12] Haruta, M.; Kobayashi, T.; Sano, H.; Yamada, N. Novel gold catalysts for the oxidation of carbon monoxide at a temperature far below 0-degrees-C. *Chem. Lett.* **1987**, 405–408.

[13] Haruta, M.; Yamada, N.; Kobayashi, T.; Iijima, S. Gold catalysts prepared by coprecipitation for low-temperature oxidation of hydrogen and of carbon monoxide. *J. Catal.* **1989**, *115*, 301–309.

[14] Hashmi, A. S. K.; Hutchings, G. J. Gold catalysis. *Angew. Chem. Int. Ed.* **2006**, *45*, 7896–7936.

[15] Aguilar-Guerrero, V.; Gates, B. C. Kinetics of CO oxidation catalyzed by supported gold: A tabular summary of the literature. *Catal. Lett.* **2009**, *130*, 108–120.

[16] Iizuka, Y.; Fujiki, H.; Yamauchi, N.; Chijiiwa, T.; Arai, S.; Tsubota, S.; Haruta, M. Adsorption of CO on gold supported on $TiO_2$. *Catal. Today* **1997**, *36*, 115–123.

[17] Iizuka, Y.; Tode, T.; Takao, T.; Yatsu, K. I.; Takeuchi, T.; Tsubota, S.; Haruta, M. A kinetic and adsorption study of CO oxidation over unsupported fine gold powder and over gold supported on titanium dioxide. *J. Catal.* **1999**, *187*, 50–58.

[18] Park, E. D.; Lee, J. S. Effects of pretreatment conditions on CO oxidation over supported Au catalysts. *J. Catal.* **1999**, *186*, 1–11.

[19] Schubert, M. M.; Hackenberg, S.; van Veen, A. C.; Muhler, M.; Plzak, V.; Behm, R. J. CO oxidation over supported gold catalysts-"inert" and "active" support materials and their role for the oxygen supply during reaction. *J. Catal.* **2001**, *197*, 113–122.

[20] Kung, H. H.; Kung, M. C.; Costello, C. K. Supported Au catalysts for low temperature CO oxidation. *J. Catal.* **2003**,

*216*, 425–432.

[21] Zhong, Z. Y.; Lin, J. Y.; Teh, S. P.; Teo, J.; Dautzenberg, F. M. A rapid and efficient method to deposit gold particles on catalyst supports and its application for CO oxidation at low temperatures. *Adv. Funct. Mater.* **2007**, *17*, 1402–1408.

[22] Perkas, N.; Zhong, Z.; Grinblat, J.; Gedanken, A. Deposition of gold particles on mesoporous catalyst supports by sono-chemical method, and their catalytic performance for CO oxidation. *Catal. Lett.* **2008**, *120*, 19–24.

[23] Zhu, Y. H.; Li, W.; Zhou, Y. X.; Lu, X. H.; Feng, X.; Yang, Z. H. Low-temperature CO oxidation of gold catalysts loaded on mesoporous $TiO_2$ whisker derived from potassium dititanate. *Catal. Lett.* **2009**, *127*, 406–410.

[24] Tanielyan, S. K.; Augustine, R. L. Effect of catalyst pretreatment on the oxidation of carbon-monoxide over coprecipitated gold catalysts. *Appl. Catal. A: Gen.* **1992**, *85*, 73–87.

[25] Hutchings, G. J.; Siddiqui, M. R. H.; Burrows, A.; Kiely, C. J.; Whyman, R. High-activity Au/CuO–ZnO catalysts for the oxidation of carbon monoxide at ambient temperature. *J. Chem Soc., Faraday Trans.* **1997**, *93*, 187–188.

[26] Solsona, B. E.; Garcia, T.; Jones, C.; Taylor, S. H.; Carley, A. F.; Hutchings, G. J. Supported gold catalysts for the total oxidation of alkanes and carbon monoxide. *Appl. Catal. A: Gen.* **2006**, *312*, 67–76.

[27] Ando, M.; Kobayashi, T.; Haruta, M. Combined effects of small gold particles on the optical gas sensing by transition metal oxide films. *Catal. Today* **1997**, *36*, 135–141.

[28] Avgouropoulos, G.; Papavasiliou, J.; Tabakova, T.; Idakiev, V.; Ioannides, T. A comparative study of ceria-supported gold and copper oxide catalysts for preferential CO oxidation reaction. *Chem. Eng. J.* **2006**, *124*, 41–45.

[29] Pillai, U. R.; Deevi, S. Room temperature oxidation of carbon monoxide over copper oxide catalyst. *Appl. Catal. B: Environ.* **2006**, *64*, 146–151.

[30] Haruta, M.; Yamada, N.; Kobayashi, T.; Iijima, S. Gold catalysts prepared by coprecipitation for low-temperature oxidation of hydrogen and carbon-monoxide. *J. Catal.* **1989**, *115*, 301–309.

[31] Zhou, S. H.; Yin, H. F.; Schwartz, V.; Wu, Z. L.; Mullins, D.; Eichhorn, B.; Overbury, S. H.; Dai, S. *In situ* phase separation of NiAu alloy nanoparticles for preparing highly active Au/NiO CO oxidation catalysts. *ChemPhysChem* **2008**, *9*, 2475–2479.

[32] Radwan, N. R. E.; Ei-Shall, M. S.; Hassan, H. M. A. Synthesis and characterization of nanoparticle $CO_3O_4$, CuO, and NiO catalysts prepared by physical and chemical methods to minimize air pollution. *Appl. Catal. A: Gen.* **2007**, *331*, 8–18.

[33] Zhang, W. X.; Tao, Y. G.; Jia, M. J.; Wu, T. H.; Li, X. M. Catalytic oxidation of CO at ambient temperature and humidity on Au/NiO prepared by using different methods. *Chem. J. Chin. Univ.* **1998**, *19*, 1317–1319.

[34] Wang, G. Y.; Zhang, W. X.; Jiang, D. Z.; Wu, T. H. CO oxidation over Au/$MeO_x$ at ambient temperature and humidity. *Acta Chim. Sinica* **2000**, *58*, 1557–1562.

[35] Wang, G. Y.; Zhang, W. X.; Cui, Y. C.; Lian, H. L.; Jiang, D. Z.; Wu, T. H. Effect of $H_2O$ on catalytic performance of $MO_x$, and Au/$MO_x$ catalysts for CO oxidation. *Chin. J. Catal.* **2001**, *22*, 408–410.

[36] Wang, D. S.; Xu, R.; Wang, X.; Li, Y. D. NiO nanorings and their unexpected catalytic property for CO oxidation. *Nanotechnol.* **2006**, *17*, 979–983.

[37] Guzman, J.; Corma, A. Nanocrystalline and mesostructured $Y_2O_3$ as supports for gold catalysts. *Chem. Commun.* **2005**, 743–745.

[38] Guzman, J.; Carrettin, S.; Fierro-Gonzalez, J. C.; Hao, Y. L.; Gates, B. C.; Corma, A. CO oxidation catalyzed by supported gold: Cooperation between gold and nanocrystalline rare-earth supports forms reactive surface superoxide and peroxide species. *Angew. Chem. Int. Ed.* **2005**, *44*, 4778–4781.

[39] Russo, N.; Fino, D.; Saracco, G.; Specchia, V. Supported gold catalysts for CO oxidation. *Catal. Today* **2006**, *117*, 214–219.

[40] Fierro-Gonzalez, J. C.; Bhirud, V. A.; Gates, B. C. A highly active catalyst for CO oxidation at 298 K: Mononuclear Au-III complexes anchored to $La_2O_3$ nanoparticles. *Chem. Commun.* **2005**, 5275–5277.

[41] Mihaylov, M.; Ivanova, E.; Hao, Y.; Hadjiivanov, K.; Knozinger, H.; Gates, B. C. Gold supported on $La_2O_3$: Structure and reactivity with $CO_2$ and implications for CO oxidation catalysis. *J. Phys. Chem. C* **2008**, *112*, 18973–18983.

[42] Mihaylov, M.; Ivanova, E.; Hao, Y.; Hadjiivanov, K.; Gates, B. C.; Knozinger, H. Oxidation by $CO_2$ of Au-0 species on $La_2O_3$-supported gold clusters. *Chem. Commun.* **2008**, 175–177.

[43] Grisel, R. J. H.; Nieuwenhuys, B. E. Selective oxidation of CO over supported Au catalysts. *J. Catal.* **2001**, *199*, 48–59.

[44] Gasior, M.; Grzybowska, B.; Samson, K.; Ruszel, A.; Haber, J. Oxidation of CO and $C_3$ hydrocarbons on gold dispersed on oxide supports. *Catal. Today* **2003**, *91–92*, 131–135.

[45] Szabo, E. G.; Hegedus, M.; Szegedi, A.; Sajo, I.; Margitfalvi, J. L. CO oxidation over Au/$Al_2O_3$ catalysts modified by MgO. *React. Kinet. Catal. Lett.* **2005**, *86*, 339–345.

[46] Bowker, M.; Nuhu, A.; Soares, J. High activity supported gold catalysts by incipient wetness impregnation. *Catal. Today* **2007**, *122*, 245–247.

[47] Sunagawa, Y.; Yamamoto, K.; Takahashi, H.; Muramatsu, A. Liquid-phase reductive deposition as a novel nano-particle synthesis method and its application to supported noble metal catalyst preparation. *Catal. Today* **2008**, *132*, 81–87.

[48] Carabineiro, S. A. C.; Silva, A. M. T.; Dražić, G.; Tavares, P. B.; Figueiredo, J. L. Gold nanoparticles on ceria supports for the oxidation of carbon monoxide. *Catal. Today* **2010**, *154*, 21–30.

[49] Carabineiro, S. A. C.; Bastos, S. S. T.; Órfão, J. J. M.; Pereira, M. F. R.; Delgado, J. J.; Figueiredo, J. L. Exotemplated ceria catalysts with gold for CO oxidation. *Appl. Catal. A: Gen.* **2010**, *381*, 150–160.

[50] Carabineiro, S. A. C.; Machado, B. F.; Bacsa, R. R.; Serp, P.; Dražić, G.; Faria, J. L.; Figueiredo, J. L. Catalytic performance of Au/ZnO nanocatalysts for CO oxidation. *J. Catal.* **2010**, *273*, 191–198.

[51] Carabineiro, S. A. C.; Silva, A. M. T.; Dražić, G.; Tavares, P. B.; Figueiredo, J. L. Effect of chloride on the sinterization of Au/$CeO_2$ catalysts. *Catal. Today* **2010**, *154*, 293–302.

[52] Santos, V. P.; Carabineiro, S. A. C.; Tavares, P. B.; Pereira, M. F. R.; Órfão, J. J. M.; Figueiredo, J. L. Oxidation of CO, ethanol, and toluene over $TiO_2$ supported noble metal catalysts. *Appl. Catal. B: Environ.* **2010**, *99*, 198–205.

[53] Carabineiro, S. A. C.; Bastos, S. S. T.; Orfao, J. J. M.; Pereira, M. F. R.; Delgado, J. J.; Figueiredo, J. L. Carbon monoxide oxidation catalysed by exotemplated manganese oxides. *Catal. Lett.* **2010**, *134*, 217–227.

[54] Available from: http://cimewww.epfl.ch/people/stadelmann/jemsWebSite/jems.html.

[55] Kraus, W.; Nolze, G. *PowderCell for Windows.* http://ccp14.minerals.csiro.au/ccp/web-mirrors/powdcell/a v/v 1/powder/e cell.html.

[56] Margitfalvi, J. L.; Fasi, A.; Hegedus, M.; Lonyi, F.; Gobolos, S.; Bogdanchikova, N. Au/MgO catalysts modified with ascorbic acid for low temperature CO oxidation. *Catal. Today* **2002**, *72*, 157–169.

[57] Guzman, J.; Gates, B. C. Catalysis by supported gold: Correlation between catalytic activity for CO oxidation and oxidation states of gold. *J. Am Chem. Soc.* **2004**, *126*, 2672–2673.

[58] Szabo, E. G.; Tompos, A.; Hegedus, M.; Szegedi, A.; Margitfalvi, J. L. The influence of cooling atmosphere after reduction on the catalytic properties of Au/$Al_2O_3$ and Au/MgO catalysts in CO oxidation. *Appl. Catal. A: Gen.* **2007**, *320*, 114–121.

[59] Choudhary, V. R.; Mulla, S. A. R.; Uphade, B. S. Oxidative coupling of methane over supported $La_2O_3$ and La-promoted MgO catalysts: Influence of catalyst−support interactions. *Ind. Eng. Chem. Res.* **1997**, *36*, 2096–2100.

[60] Ko, E. Y.; Park, E. D.; Seo, K. W.; Lee, H. C.; Lee, D.; Kim, S. A comparative study of catalysts for the preferential CO oxidation in excess hydrogen. *Catal. Today* **2006**, *116*, 377–383.

[61] Carabineiro, S. A. C.; Silva, A. M. T.; Dražić, G.; Figueiredo, J. L. Analytical electron microscopy of gold nanoparticles on ceria, titania, and ceria-titania materials. In *Microscopy: Science, Technology, Applications and Education, Formatex Microscopy Book series*. Formatex Research Center, 2010.

[62] Sakurai, H.; Tsubota, S.; Haruta, M. Hydrogenation of CO over gold supported on metal oxides. *Appl. Catal. A: Gen.* **1993**, *102*, 125–136.

[63] Arena, F.; Frusteri, F.; Parmaliana, A.; Giordano, N. On the reduction of NiO forms in magnesia supported catalysts. *React. Kinet. Catal. Lett.* **1990**, *42*, 121–126.

[64] Parmaliana, A.; Arena, F.; Frusteri, F.; Giordano, N. Temperature-programmed reduction study of NiO–MgO interactions in magnesia-supported Ni catalysts and NiO–MgO physical mixture. *J. Chem Soc., Faraday Trans.* **1990**, *86*, 2663–2669.

[65] Kotsev, N. K.; Ilieva, L. I. Determination of nons-toichiometric oxygen in NiO by temperature-programmed reduction. *Catal. Lett.* **1993**, *18*, 173–176.

[66] Li, C. P.; Chen, Y. W. Temperature-programmed-reduction studies of nickel-oxide alumina catalysts—Effects of the preparation method. *Thermochim. Acta* **1995**, *256*, 457–465.

[67] Bellido, J. D. A.; Assaf, E. M. Effect of the $Y_2O_3$–$ZrO_2$ support composition on nickel catalyst evaluated in dry reforming of methane. *Appl. Catal. A: Gen.* **2009**, *352*, 179–187.